



# Nanoscale Structure and Dynamics of Model Membrane Lipid Raft Systems, Studied by Neutron Scattering Methods

Delaram Ahmadi<sup>1</sup>, Katherine C. Thompson<sup>2</sup>, Victoria García Sakai<sup>3</sup>, Ralf Schweins<sup>4</sup>, Martine Moulin<sup>5,6</sup>, Michael Haertlein<sup>5,6</sup>, Gernot A. Strohmaier<sup>7,8</sup>, Harald Pichler<sup>7,9</sup>, V. Trevor Forsyth<sup>5,6,10,11,12</sup>, David J. Barlow<sup>1</sup>, M. Jayne Lawrence<sup>1</sup> and Fabrizia Foglia<sup>13\*</sup>

<sup>1</sup>Division of Pharmacy and Optometry, School of Health Sciences, Stopford Building, University of Manchester, Manchester, United Kingdom, <sup>2</sup>Department of Biological Sciences and Institute of Structural and Molecular Biology, Birkbeck University of London, London, United Kingdom, <sup>3</sup>ISIS Neutron and Muon Facility, Science & Technology Facilities Council, Rutherford Appleton Laboratory, Didcot, United Kingdom, <sup>4</sup>Institut Laue-Langevin, Grenoble, France, <sup>5</sup>Life Sciences Group, Carl-Ivar Brändén Building, Institut Laue-Langevin, Grenoble, France, <sup>6</sup>Partnership for Structural Biology, Grenoble, France, <sup>7</sup>Austrian Centre of Industrial Biotechnology GmbH, Graz, Austria, <sup>8</sup>Institute of Organic Chemistry, NAWI Graz, Graz University of Technology, Graz, Austria, <sup>9</sup>Institute of Molecular Biotechnology, NAWI Graz, BioTechMed Graz, Graz University of Technology, Graz, Austria, <sup>10</sup>Faculty of Natural Sciences, Keele University, Staffordshire, United Kingdom, <sup>11</sup>Faculty of Medicine, Lund University, Lund, Sweden, <sup>12</sup>LINXS Institute of Advanced Neutron and X-Ray Science, Lund, Sweden, <sup>13</sup>Department of Chemistry, Christopher Ingold Laboratories, University College London, London, United Kingdom

## OPEN ACCESS

### Edited by:

Arlette R. C. Bajon,  
San Diego State University,  
United States

### Reviewed by:

Oskar Engberg,  
University Hospital Leipzig, Germany  
Eneida De Paula,  
State University of Campinas, Brazil

### \*Correspondence:

Fabrizia Foglia  
f.foglia@ucl.ac.uk

### Specialty section:

This article was submitted to  
Soft Matter Physics,  
a section of the journal  
Frontiers in Physics

**Received:** 28 January 2022

**Accepted:** 29 March 2022

**Published:** 27 April 2022

### Citation:

Ahmadi D, Thompson KC, García Sakai V, Schweins R, Moulin M, Haertlein M, Strohmaier GA, Pichler H, Forsyth VT, Barlow DJ, Lawrence MJ and Foglia F (2022) Nanoscale Structure and Dynamics of Model Membrane Lipid Raft Systems, Studied by Neutron Scattering Methods. *Front. Phys.* 10:864746. doi: 10.3389/fphy.2022.864746

Quasi-elastic neutron scattering (QENS) and small angle neutron scattering (SANS), in combination with isotopic contrast variation, have been used to determine the structure and dynamics of three-component lipid membranes, in the form of vesicles, comprising an unsaturated [palmitoyl-oleoyl-phosphatidylcholine (POPC) or dioleoyl-phosphatidylcholine (DOPC)], a saturated phospholipid (dipalmitoyl-phosphatidylcholine (DPPC)), and cholesterol, as a function temperature and composition. SANS studies showed vesicle membranes composed of a 1:1:1 molar ratio of DPPC:DOPC:cholesterol and a 2:2:1 molar ratio of DPPC:POPC:cholesterol phase separated, forming lipid rafts of ~18 and ~7 nm diameter respectively, when decreasing temperature from 308 to 297 K. Phase separation was reversible upon increasing temperature. The larger rafts observed in systems containing DOPC are attributed to the greater mis-match in lipid alkyl chains between DOPC and DPPC, than for POPC and DPPC. QENS studies, over the temperature range 283–323K, showed that the resulting data were best modelled by two Lorentzian functions: a narrow component, describing the “in-plane” lipid diffusion, and a broader component, describing the lipid alkyl chain segmental relaxation. The overall “in-plane” diffusion was found to show a significant reduction upon increasing temperature due to the vesicle membranes transitioning from one containing rafts to one where the component lipids are homogeneously mixed. The use of different isotopic combinations allowed the measured overall reduction of in-plane diffusion to be understood in terms of an increase in diffusion of the saturated DPPC lipid and a corresponding decrease in diffusion of the unsaturated DOPC/POPC lipid. As the rafts are considered to be composed principally of saturated lipid and cholesterol, the breakdown of rafts decreases the exposure of the DPPC to cholesterol whilst increasing the exposure of

cholesterol to unsaturated lipid. These results show the sensitivity of lipid diffusion to local cholesterol concentration, and the importance of considering the local, rather than the global composition of a membrane when understanding the diffusion processes of lipids within the membrane. The novel combination of SANS and QENS allows a non-intrusive approach to characterize the structure and dynamics occurring in phase-separated model membranes which are designed to mimic the lateral heterogeneity of lipids seen in cellular membranes—a heterogeneity that can have pathological consequences.

**Keywords:** QENS, SANS, lipid rafts, lipid, multi-component systems

## 1 INTRODUCTION

Biological membranes are critical to the integrity and activity of cells: they not only provide for a physical compartmentalisation of their internal metabolic processes, but also afford the means by which they are able to regulate the import, export, and exchange of substances, and mediate the transduction of chemical signals received extracellularly [1, 2]. In the Singer and Nicholson model proposed in 1972, they were viewed as a disordered mosaic in which bilayer lipids and embedded proteins move freely by lateral diffusion, with the lipids considered to play only a passive role—providing the building blocks to constitute the barrier separating the cell's internal and external environments.

It was later shown that cell membranes also possess regions where the lipids are much more tightly packed, forming highly organised micro-domains of around 100 nm in diameter [3]. These micro-domains—also referred to as lipid rafts—were shown to be composed of phospholipid, cholesterol, and sphingolipids [4, 5] and, as a consequence of their lateral segregation and/or demixing behaviour, were demonstrated to exist as liquid-ordered ( $l_o$ ) islands of reduced fluidity that co-exist within the “loosely packed” liquid-disordered ( $l_d$  phase), frequently unsaturated, phospholipids present in the bulk of the membrane [2]. These  $l_o$  phase raft platforms exist by virtue of cholesterol's propensity to form condensed molecular complexes with, for example, long chain saturated phospholipids, such that its local concentration rises above ~20%, creating zones with an almost binary lipid composition [6–8]. For recent reviews covering the history, composition, and mesoscale organisation of lipid rafts, the reader is referred to Gori [9], Lu and Fairn [10] and Sezgin et al [11].

As regards their functions within biological systems, lipid rafts are known to play major roles in membrane protein trafficking, in signal transduction, and in mediating the cellular entry and exit of pathogens [12, 13]. The dense organisation of their lipids and proteins also leads to enhanced protein-protein interaction, and can result in accelerated signal transduction and enhanced enzyme activity [12].

The clustering of rafts has also been implicated in the pathogenesis of microbial infections [14] and they are thus relevant to our understanding of the development and spread of infectious diseases. Their formation and distribution within cell membranes are shown to be pertinent to cardiovascular disease [15], ageing and neurodegenerative diseases [16], inflammation [17] and cancer [18–20]. Further knowledge and

understanding of lipid raft composition and dynamic behaviour, could thus offer the potential to facilitate development of future therapies to treat a diverse range of pathological conditions.

Studies that have focused on the structure and physico-chemical properties of lipid rafts have generally involved *in-silico* modelling and/or experimental studies utilising model systems [21–31]. Since lipids have different molecular configurations depending on temperature, structural studies have been performed to investigate the formation of rafts in lipid vesicle membranes as a function of temperature and raft composition [21–23, 30–32]. Despite the temperature dependence of lipid mixtures witnessed in *in-vitro* systems [30, 32], fundamental questions remain about the physical mechanisms that govern the formation, size, and stability of these  $l_o$  phase lipid “platforms”, especially those formed *in vivo*, and there has been very little experimental research performed to probe the dynamic behaviour of lipid raft systems at the molecular level.

In the work reported here we sought to rectify this deficiency by employing quasi-elastic neutron scattering (QENS) to explore the dynamics of lipids on a picosecond timescale following temperature-induced lipid raft formation in ternary lipid vesicles (widely studied by others [33–38]) composed of dipalmitoylphosphatidylcholine (DPPC), cholesterol (Chol) and either palmitoyl- or dioleoyl-phosphatidylcholine (POPC and DOPC, respectively). Complementary structural studies of the systems were also performed using small angle neutron scattering (SANS) and dynamic light scattering (DLS) experiments.

The novel combination of SANS and QENS methodology deployed here is shown to provide an informative and non-intrusive (non-perturbing, reporter-free) way in which to characterize the structure and dynamics of phase segregated model membrane systems at the molecular level. The methodology might thus be used to explore the behaviour of model membranes with compositions more closely designed to mimic the lateral heterogeneity seen in cellular membranes—a heterogeneity that often carries pathological consequences.

## 2 MATERIALS AND METHODS

### 2.1 Materials

All protiated components and partially-deuterated phospholipids and cholesterol (e.g.  $d_7$ -Chol) were purchased from Avanti Polar

**TABLE 1** | Sample characteristics post preparation.

Lipid composition	Molar ratio	Apparent hydrodynamic diameter (nm):	Concentration (mg/ml)	Solvent	Technique
<i>d</i> <sub>75</sub> -DPPC: <i>h</i> -DOPC: <i>d</i> <sub>7</sub> -Chol	1:1:1	120 ± 15	30	D <sub>2</sub> O	QENS
<i>d</i> <sub>62</sub> -DPPC: <i>h</i> -DOPC: <i>h</i> -Chol	1:1:1	127 ± 14	10	D <sub>2</sub> O:H <sub>2</sub> O	SANS
<i>d</i> <sub>62</sub> -DPPC: <i>h</i> -DOPC: <i>h</i> -Chol	15:60:25	129 ± 14	10	D <sub>2</sub> O:H <sub>2</sub> O	SANS
<i>h</i> -DPPC: <i>h</i> -POPC: <i>h</i> -Chol	2:2:1	137 ± 16	30	D <sub>2</sub> O	QENS
<i>d</i> <sub>75</sub> -DPPC: <i>h</i> -POPC: <i>d</i> <sub>46</sub> -Chol	2:2:1	139 ± 14	30	D <sub>2</sub> O	QENS
<i>d</i> <sub>62</sub> -DPPC: <i>h</i> -POPC: <i>h</i> -Chol	2:2:1	132 ± 13	10	D <sub>2</sub> O:H <sub>2</sub> O	SANS

Lipids (Alabaster, AL, United States). Perdeuterated cholesterol was produced in the Deuteration Laboratory platform of the Life Sciences group [39] at the Institut Laue Langevin (ILL) in Grenoble, France, using a lipo-engineered cholesterol producing *Pichia pastoris* strain CBS7435Δhis4Δku70 Δerg5::pPpGAP-ZeocinTM-[DHCR7]Δerg6::pGAP-G418 [DHCR24] [40]. Following adaptation to growth in deuterated minimal medium, cells were grown in a high cell density fermenter culture. Purification was carried out by HPLC on a NUCLEODUR® 100–10 C18ec column (Macherey-Nagel, Düren, Germany) using an isocratic mixture consisting of acetonitrile/methanol (9:1) at a flow rate of 20 ml/min [41]. Deuterated cholesterol made in this way is now widely used in neutron scattering and related studies [42, 43].

## 2.2 Methods

### 2.1.1 Vesicle Preparation

Three types of small unilamellar vesicles were prepared: 1) DPPC:DOPC:Chol in molar ratio 1:1:1 (raft forming mixture); 2) DPPC:DOPC:Chol molar ratio 15:60:25 (non-raft forming mixture) and 3) DPPC:POPC:Chol molar ratio 2:2:1 (raft forming mixture). The DPPC:DOPC:Chol 1:1:1 and DPPC:POPC:Chol 2:2:1 mixtures were used to study the dynamics in rafts of differing sizes [38]. Different isotopic forms and concentration of the vesicles were prepared for the SANS and QENS study as shown in **Table 1**. Owing to the differences between the neutron scattering cross sections of the lipids (as a result of the difference in interactions, coherent and incoherent, between hydrogen and deuterium:  $\sigma_{coh}H = 1.76$  barn,  $\sigma_{coh}D = 5.59$  barn,  $\sigma_{inc}H = 79.74$  barn;  $\sigma_{inc}D = 2.01$  barn), selectively deuterated samples were used in order to make ‘invisible’ certain components in the mixtures whilst highlighting others. The contrast combination requirements for the two techniques used, SANS and QENS are slightly different. For QENS the use of perdeuterated components within the lipid dispersion makes it possible to ‘hide’ a molecule’s dynamics and thereby highlight the dynamics related to the fully protiated component. Note here, that due to the limited availability of perdeuterated cholesterol, experiments were also performed using partially deuterated chol (as in the case of *d*<sub>75</sub>-DPPC:*h*-DOPC:*d*<sub>7</sub>-Chol 1:1:1). For the same reason and in order to “hide” the solvent dynamics, the lipid dispersions for QENS were prepared in D<sub>2</sub>O (if instead H<sub>2</sub>O were used as the solvent, its signal would dominate the scattering profile). In the case of the SANS experiments, the solvent used to prepare the vesicles was

selected to have the same scattering length density (SLD) as the lipids comprising the vesicle (assuming the lipids to be homogeneously mixed at high temperatures). Therefore any phase separation of the lipids within the vesicle membranes as a result of a reduction in temperature would lead to the formation of regions of differing SLD’s that are no longer matched to the SLD of the solvent.

To prepare the vesicles, the lipids were weighed in accordance with the desired molar ratio, correcting for deuteration appropriate, and dissolved in chloroform (spectroscopic grade, Fluka United Kingdom, Ltd., Dorset, United Kingdom). The solvent was then evaporated to dryness using a BUCHI 461 rotary evaporator and the resultant dry lipid film hydrated with either D<sub>2</sub>O (99.7% D; Aldrich, United Kingdom, Ltd., Dorset) or a D<sub>2</sub>O:H<sub>2</sub>O mixture; where the SLD of the D<sub>2</sub>O:H<sub>2</sub>O dispersion medium was selected to match the “average” SLD of the ternary lipid mixture assuming ideal mixing (termed as “on-contrast”). For the 1:1:1 molar ratio mixture of *d*<sub>62</sub>-DPPC:*h*-DOPC:*h*-Chol, the calculated SLD was  $2.29 \times 10^{-6} \text{ \AA}^{-2}$  and so a mixture of H<sub>2</sub>O 5.8662 g and D<sub>2</sub>O 4.5568 g was used. Samples were prepared at two different total lipid concentrations, namely 10 and 30 mg ml<sup>-1</sup> for SANS and QENS, respectively. Note, that for our SANS studies the total lipid concentration of 10 mg ml<sup>-1</sup> had been optimised by earlier studies to enable the ready production of the unilamellar vesicles necessary for the study, whilst at the same time yielding sufficient neutron scattering signal. The higher total lipid concentration used for the QENS study is necessary to increase the statistical accuracy of the data. Note that additional broadening due to the diffusion of the centre of mass of whole vesicles can be neglected.

To produce unilamellar vesicles of uniform and defined size from the highly concentrated lipid suspensions prepared here, the lipid suspension was firstly sonicated; the vesicles were then extruded under pressure (compressed nitrogen gas at a pressure of 15 bar) through polycarbonate filters of 100 nm pore (Nuclepore Track-Etch membrane). To aid the extrusion process, the temperature of the extruder was set at 326 K, above the transition temperature of the highest melting point lipid, namely  $\sim 314 \pm 1$  K for DPPC, to ensure all the lipids were in a fluid state when extruded. The vesicle suspensions were filtered an odd number of times until the desired mean vesicle diameter size of about 120 nm was achieved, suggesting the formation of a predominately unilamellar population of vesicles. **Table 1** gives the mean apparent hydrodynamic diameter for each type of vesicle prepared (with a measured polydispersity of  $\sim 0.15$  in

all cases); the data were measured on a diluted vesicle dispersion (x100) using Dynamic Light Scattering (DLS; NanoBrook Zeta Potential Analyzer, Brookhaven Instruments Corporation, Long Island, NY) over 3 days to ensure that the dispersions were stable with respect to their size (at ambient temperature), for the length of time required to complete the neutron scattering experiments.

### 2.1.2 Small Angle Neutron Scattering

SANS measurements were performed on the D11 instrument at the Institut Laue Langevin (ILL) in Grenoble, France [44]. Scattering intensities were measured with a 2-D  $^3\text{He}$ -detector consisting of  $128 \times 128$  pixels of  $7.5 \times 7.5 \text{ mm}^2$  size. Measurements were performed at a wavelength of  $5 \text{ \AA}$  with a 9% full width at half maximum (FWHM), using 4 and 28 m sample-detector distances to access scattering vectors ( $Q = (4\pi/\lambda) \sin(\theta)$ ) in the range  $0.0025\text{--}0.2 \text{ \AA}^{-1}$ . Transmissions were measured at 28 m with the attenuated direct beam. Samples were acquired in quartz cuvettes with 1 mm path length and measured at either  $308$  or  $279 \pm 0.1 \text{ K}$ , using a copper sample holder for precise temperature control. Absolute intensities and detector efficiency were determined by using a 1 mm  $\text{H}_2\text{O}$  sample as secondary calibration standard, which is cross-calibrated against polystyrene h-/d- polymer blends. The differential scattering cross section of a 1 mm  $\text{H}_2\text{O}$  sample at  $5 \text{ \AA}$  on D11 is  $0.929 \text{ 1/cm}$ . The empty cell and either  $\text{D}_2\text{O}$  or the appropriate  $\text{H}_2\text{O}:\text{D}_2\text{O}$  solvent mixture were also recorded to properly reduce the raw data. Data reduction was performed using the facility-provided LAMP software [45].

Model-fitting of the SANS profiles was carried out using Sasview [46], employing either a simple power law model or a model combining a power law and a Broad/Lorentzian peak model.

### 2.1.3 Quasi-Elastic Neutron Scattering

QENS measurements were conducted using the IRIS spectrometer [47] at the ISIS Neutron and Muon Facility (Harwell, Oxford, United Kingdom). Samples were loaded into aluminum annular cans of a neutron path length of  $0.5 \text{ mm}$  to ensure a sample transmission of 90%. Elastic fixed window scans (EFWS) were conducted over the temperature range  $283\text{--}323 \pm 0.1 \text{ K}$ ; measurements were taken in increments of  $3 \pm 0.1 \text{ K}$ . Scans were conducted in both heating and cooling modes to ensure that no hysteresis was present. EFWS were used to locate the phase transition temperature range as well as to discriminate the temperature at which the dynamics enters the timescale accessible to the spectrometer; this allows specific temperatures to be selected for further investigation by QENS. Scattering profiles were then recorded with an energy resolution of  $17.5 \mu\text{eV}$ , using the PG002 analyser crystal set-up, investigating dynamics in the picosecond timescale, at temperatures of  $283, 288, 298$  and  $323 \pm 0.1 \text{ K}$ . Raw data were normalized to incoming neutron flux and corrected for detector efficiency, by direct comparison with the purely incoherent signal scattered from a vanadium standard. The double differential cross section was then converted into the corresponding dynamic structure factor  $S(Q, \omega)$ . Detectors were grouped to provide  $\sim 12$  spectra and the energy binned into constant  $5 \mu\text{eV}$  steps.

Additional normalization steps, such as removing the signal associated with the empty can and from an appropriately weighted spectrum of the  $\text{D}_2\text{O}$  solvent, as well as full data analysis were carried out directly on the  $S(Q, \omega)$  spectra using either Mantid [48] or Origin 2019b. Each Q-slice was analysed using a built-in least squares algorithm accounting for the instrumental energy resolution along with up to two Lorentzian functions.

### 2.1.4 Analysis of QENS Data

QENS measurements provide data on the broadening, measured as an energy transfer ( $\hbar\omega$ ) that appears around the elastic scattering signal, resulting from dynamical relaxation processes in the system. The latter are mainly due to local motions and/or diffusional events. More specifically, the scattering function is composed of both coherent and incoherent scattering terms (owing to the nature of the neutron-nucleus interactions), enabling the computation of the spatio-temporal correlations between identical nuclei ( $S_{inc}$ ) and the static and dynamic correlations of distinct nuclei ( $S_{coh}$ ) according to [49]:

$$S(Q, \omega) = S_{inc}(Q, \omega) + S_{coh}(Q, \omega) \quad (1)$$

The elastic signal is modelled using the instrumental resolution obtained from the vanadium standard. The broadening is modelled using Lorentzian functions, and is analysed by examining the correlation of the linewidth ( $\Gamma$ , HWHM) that determines the relaxation time ( $\tau$ ) for the process involved. In its simplest form, the measured signal, which is typically dominated by that of hydrogen, provides correlations of single H atoms, and can be deconvoluted into vibrational, rotational and translational components:

$$S_{inc}(Q, \omega) = S_V(Q, \omega) \otimes S_R(Q, \omega) \otimes S_T(Q, \omega) \quad (2)$$

In the case of isotropic, harmonic vibrations, the first term can be written as:

$$S_{vib}(Q, \omega) = e^{-Q^2 \langle u^2 \rangle / 3} \quad (3)$$

where  $\langle u^2 \rangle$  is the mean square displacement.

It is worth noticing that the “experimental scattering function” (e.g.  $S(Q, \omega)_{measured}$ ) contains an implicit “resolution effect” ( $R(\omega)$ ), which translates into specific dynamics being “visible or not” within the time-scale accessible by a specific instrument. Note that the “measured scattering function” (e.g.  $S(Q, \omega)_{measured}$ ) is given by the “real scattering function” (e.g.  $S(Q, \omega)_{real}$ ) convoluted with  $R(Q, \omega)$ .

Diffusional processes result in a dispersive  $\Gamma(Q^2)$  relation [49–53] from which a diffusion coefficient can be extracted, and in general terms can be described with a Lorentzian function:

$$S(Q, \omega) = \frac{1}{\pi} \frac{\Gamma}{\omega^2 + (\Gamma)^2} \quad (4)$$

The dynamics in lipidic systems is a complex mix of processes spanning a wide range of time scales. Generally speaking there are two main processes occurring over different timescales, described as “rattling-in-a-cage”, where a lipid molecule can be thought of as moving around within a cage formed by the surrounding lipids,

and “random-walk-like”, where a lipid molecule moves out of its cage to occupy a new space within the bilayer and its original location is occupied by a different lipid molecule. However, little is known about the mechanism of how lipids actually diffuse, especially in raft-like domains or in real cellular entities.

Based on the timescale probed by the QENS instrument used here, in the order of picoseconds, we use a jump diffusion model to best describe the “in-plane” lipid diffusion:

$$\Gamma_T = \frac{D_t Q^2}{1 + Q^2 D_t \tau_0} \quad (5)$$

where  $D_t$  is the translational diffusion coefficient and  $\tau_0$  is a residence time [49–53]. This model allows us to describe how the lipid molecule moves out of its cage [53].

When non-diffusive phenomena are involved, such as in the case of spatial confinement, **Eq. 4** becomes:

$$S(Q, \omega) = A_0(Q, T)\delta(\omega) + (1 - A_0(Q, T)) \frac{1}{\pi} \frac{\Gamma_T}{\omega^2 + (\Gamma_T)^2} \quad (6)$$

where  $A_0(Q, T)$  is the so-called elastic incoherent structural factor (EISF) and  $\delta(\omega)$  is the delta function representing the elastic peak (which accounts for all immobile hydrogen atoms in the system).

Scattering profiles were modelled following the approach proposed by Sharma et al. [54–56].

$$S_{ves}(Q, \omega) = A(Q)L_{lat}(\Gamma_{lat}, \omega) + (1 - A(Q))L_{tot}(\Gamma_{tot}, \omega) \quad (7)$$

$$S_{ves}(Q, \omega) = S_{lat}(Q, \omega) \otimes S_{int}(Q, \omega) \quad (8)$$

where  $S_{ves}(Q, \omega)$  represents the scattering function for the entire system, and contains the contributions from the lateral and internal motions of the lipid molecules;  $L_{tot}(\Gamma_{tot}, \omega)$ , represents a superposition of the lateral and internal motions of the lipid molecules.

Here, the EISF was modelled using a modified version of the Volino/Dianoux model [57] originally used to describe “diffusion inside a sphere”, as proposed by Carpentier et al. [58]. The model describes the lipid as having a linearly varying radius for the diffusion volumes along the lipid length. This modification is based on the consideration that hydrogen atoms along the lipid tails could experience mobilities over different spatial extents and, mathematically, is expressed as:

$$A_0(Q, T) = \frac{1}{N} \sum_{n=1}^N \left\{ \frac{3j_1(QR_n)}{QR_n} \right\}^2 \quad (9)$$

where

$$R_n = \frac{n-1}{N-1} [R_N - R_1] + R_1 \quad (10)$$

$N$  stands for the total number of atoms in the chain to which hydrogen atoms are bound and the index  $n$  starts with the carbon atom the closest to the oxygen of the phosphorus group, which connects the lipid chains with the head group;  $R_n$  is, therefore, the radius of the diffusion volume for the corresponding hydrogen atoms. **Eq. 9** has been implemented considering all the unique atoms in the lipid chain and head groups; and has further accounted for  $\text{CH}_2$  and  $\text{CH}_3$  dynamics in cholesterol. Each

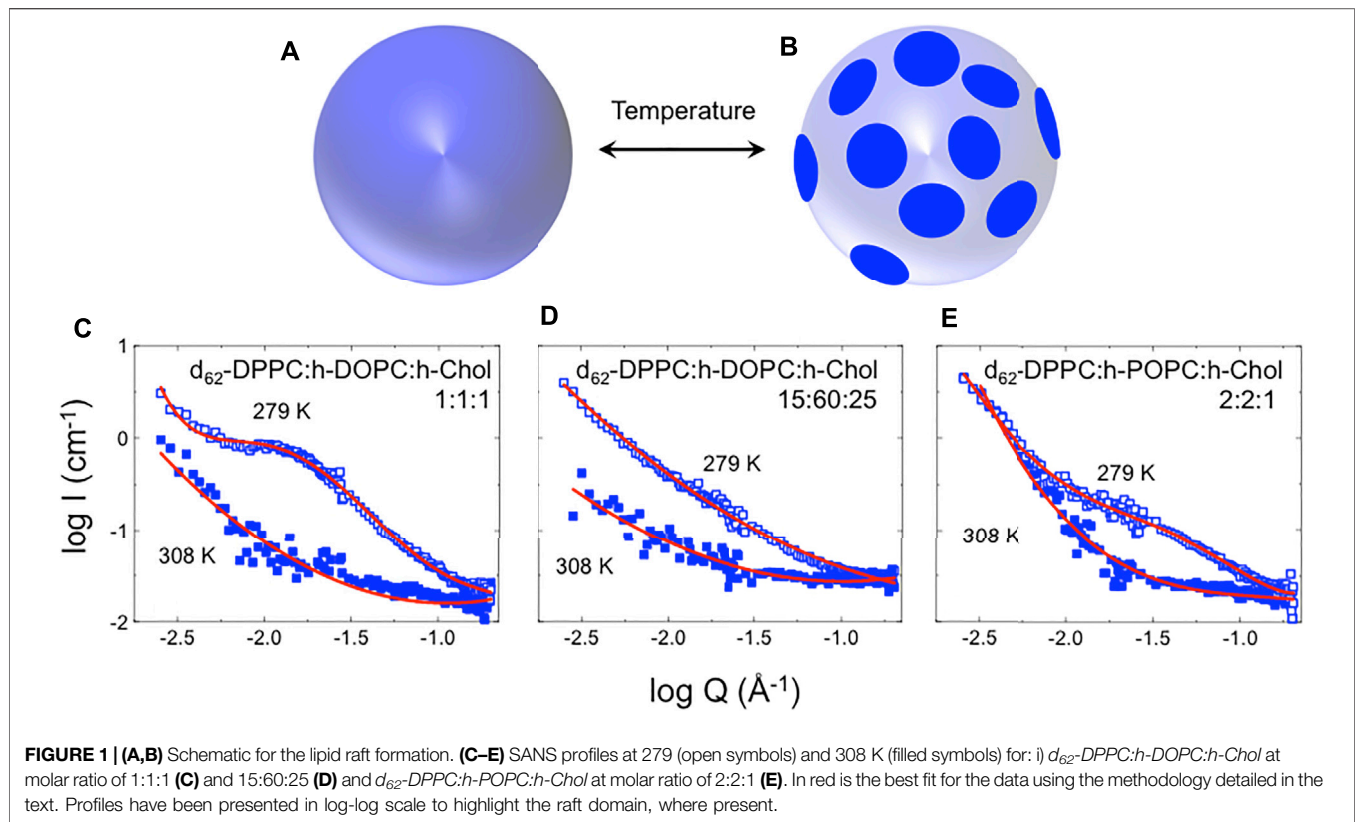
contribution has been weighted and then summed. For the DPPC:POPC:Chol 2:2:1 mixture, the partially deuterated QENS sample was first analysed to model only the POPC dynamics. The resulting parameters were then used to constrain the analysis of POPC in the fully protiated sample and, therefore, to allow the dynamics of the DPPC and cholesterol to be established. A similar approach was used to model the DPPC:DOPC:Chol 1:1:1 system, where the dynamics of ( $d_{75}$ ) DPPC was assumed to be almost invisible, allowing  $d_7$ -Chol to be modelled accounting for the dynamics of  $-\text{CH}_2$  in the chain.

## 3 RESULT AND DISCUSSION

### 3.1 Evidence of Raft Formation

SANS was used to provide evidence of the absence or presence of lipid rafts in small unilamellar vesicles as a function of lipid composition and temperature. The three lipid mixtures of differing composition and molar ratios, namely DPPC:DOPC:Chol molar ratio 1:1:1, DPPC:POPC:Chol molar ratio 2:2:1 and DPPC:DOPC:Chol molar ratio 15:60:25 (**Table 1**) were investigated, with each sample studied at  $279$  and  $308 \pm 0.1$  K. These particular compositions were selected on the basis of our own preliminary studies and those of others reported in the literature, which suggest that at  $\sim 300$  K the lipids within the vesicle membranes laterally phase segregate. In these studies, the aqueous medium used for dispersion of the vesicles was prepared so as to match the mean SLD of the ternary lipid mixture. When the lipids are homogeneously dispersed within the vesicle bilayer, i.e., when there is no lateral separation of the lipids (and thus no raft formation), as shown in **Figure 1A**, there will be negligible difference between the SLD of the vesicle lamellae and solvent. Under these conditions, little or no neutron scattering is expected from the sample—a condition referred to as “on-contrast”. When the lipids in the vesicle bilayer undergo a phase separation or “demixing”—a condition typically induced by reducing the experimental temperature such that some lipids are in the fluid state (here POPC/DOPC) and others (here DPPC) are in the gel phase—spatial differences in lipid composition occur and differences in SLD between the dispersion and the medium are observed (**Figure 1B**). Under these conditions an increase in scattering intensity is observed—a condition termed “off-contrast”.

The SANS profiles for the various vesicle preparations that were recorded at the higher experimental temperature of  $308 \pm 0.1$  K showed very little scattering, thereby confirming that the mean SLD of the vesicle lamellae had been well-matched by the SLD of the  $\text{H}_2\text{O}/\text{D}_2\text{O}$  mixture comprising the dispersion medium. The rise in  $I(Q)$  that is seen at low  $Q$  arises because of Porod scattering, due to the small difference in SLD that remains between the lipid acyl chains and the solvent (ca.  $2.6 \times 10^{-6} \text{ \AA}^{-1}$  vs. ca.  $2.3 \times 10^{-6} \text{ \AA}^{-1}$ ), with the wet/hydrated lipid phosphocholine headgroups being effectively invisible in the solvent (having an SLD of ca.  $2.2 \times 10^{-6} \text{ \AA}^{-1}$ ). Given the low-level scattering seen for these systems (being little higher than background), the model-fitting of the SANS profiles measured at  $308 \pm 0.1$  K [59–61] was performed using a simple power law

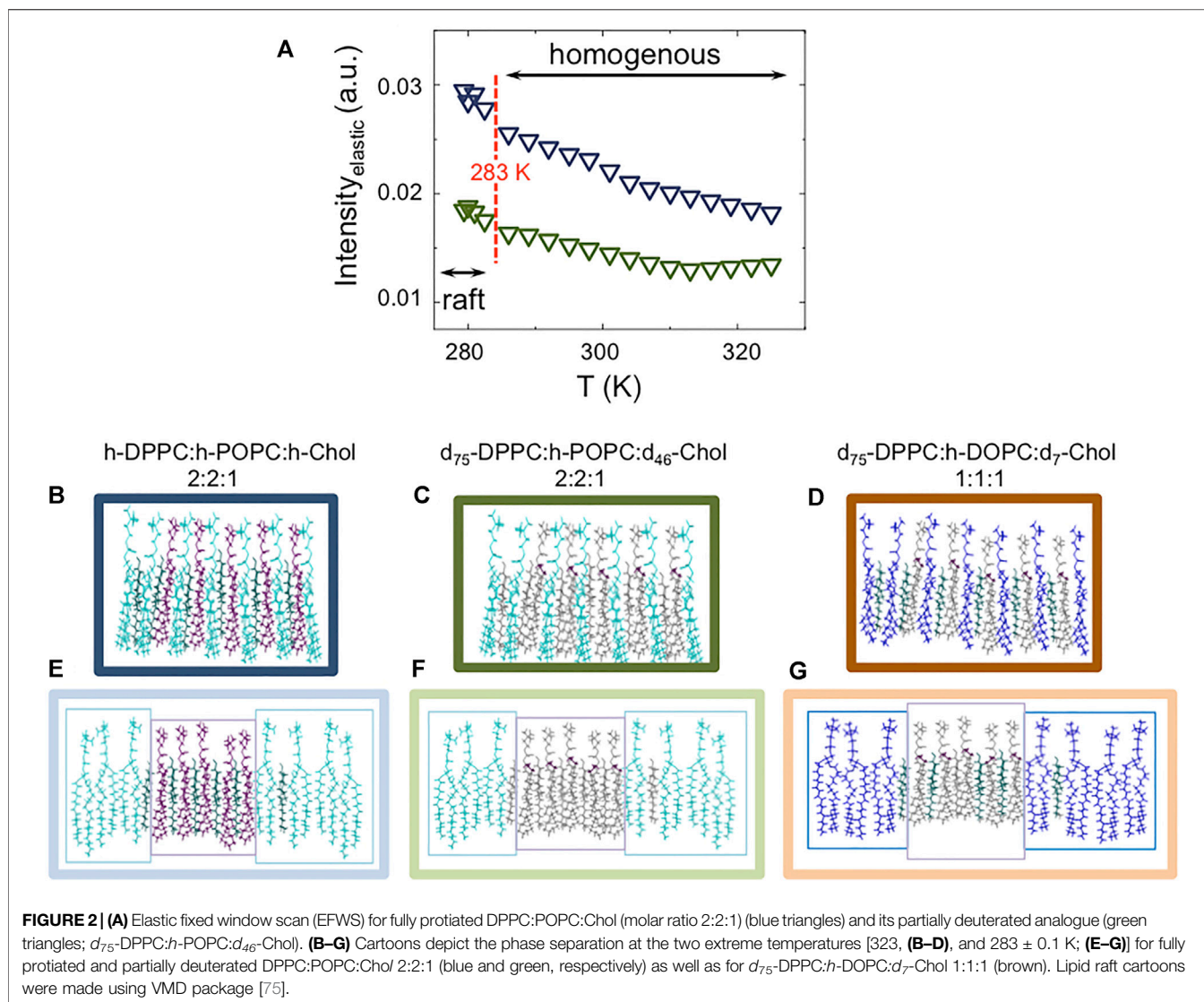


function—with the fitted exponent, thence providing a description of the interface between the dispersed (lipid lamellae) and the continuous (aqueous) phases. The values of the fitted power law (Porod) exponent ( $n$ ), were obtained as  $2.55 \pm 0.15$ ,  $2.54 \pm 0.06$ , and  $1.97 \pm 0.15$  for the vesicles prepared from 1:1:1 DPPC:DOPC:Chol, 2:2:1 DPPC:POPC:Chol and 15:60:25 DPPC:DOPC:Chol, respectively. These exponent values (each ca. 2) are characteristic of lamellae [62] and the values for the two raft-forming systems (being around 2.5) indicate roughened surfaces, while that for the non-raft forming system (being closer to 2) indicates a more smooth surface [62].

In two of the compositions studied, namely the 1:1:1 molar ratio of DPPC:DOPC:Chol and the 2:2:1 molar ratio of DPPC:POPC:Chol molar ratio 2:2:1, decreasing the temperature to  $279 \pm 0.1$  K resulted in the appearance of a broad peak in the scattering curve, indicative of the formation of lipid domains/rafts (**Figures 1C,E**). In contrast, in the case of the 15:60:25 molar ratio vesicle suspension of DPPC:DOPC:Chol (**Figure 1D**), no broad peak was observed, indicative of the absence of lipid raft formation at the experimental temperature. As found when modelling the SANS data recorded at the higher temperature of  $308 \pm 0.1$  K, it was possible to model the data obtained for the 15:60:25 DPPC:DOPC:Chol vesicles at the lower temperature using only a power law function with an exponent,  $n = 1.8 \pm 0.05$  (as compared with the exponent of  $1.97 \pm 0.15$  determined at the higher temperature of  $308 \pm 0.1$  K). In contrast, in order to model the emergence of the broad peak in the SANS profiles of the other two vesicle preparations—the formation of this peak being

attributed to domain formation [46]—a mixed model comprising Porod and Lorentzian components was used. The data were well modeled obtaining Lorentz lengths of  $87.2 \pm 1.5$  and  $34.1 \pm 1.9$  Å for the 1:1:1 DPPC:DOPC:Chol and 2:2:1 DPPC:POPC:Chol vesicles respectively, suggesting the appearance of domains of  $\sim 18$  and 7 nm across, with the fitted Porod exponent of  $2.5 \pm 0.1$  again indicating a rough interface between the continuous and disperse phases. It should be noted that the effects of temperature on raft formation are completely reproducible in that repeated heating and cooling cycles cause the domains to disappear and reform. Furthermore (although not shown here) the thickness of the vesicle bilayers, determined by SANS studies on vesicles dispersed in 100%  $D_2O$  at 308 and  $279 \pm 0.1$  K, i.e., off-contrast (well modelled assuming a mixture of isolated/single infinite planar lamellar sheets) was identical irrespective of temperature, showing that the vesicles maintained their structure upon decreasing the temperature.

The size of the domains or rafts determined here are consistent with the data obtained for similar three-component systems investigated by SANS and MD simulations [24, 31]. Additionally, the differences in the sizes of the rafts with differing lipid composition agree with the findings from previous studies wherein the sizes of the lipid domains were correlated with a mis-match in the lengths of the lipid hydrocarbon chains [35], as well as differences in line tension [63]. Furthermore, our results are also in agreement with the results presented by Zhao et al. [64] where the presence of either POPC or DOPC in a ternary mixture with sphingomyelin and



cholesterol gave rise to domains of different sizes. The difference in domain size between lipid mixtures containing POPC vs. those containing DOPC, could relate to the differing interaction of cholesterol with the lipids [65, 66]. Microsecond molecular dynamics simulations indicate that cholesterol interacts more favourably with saturated lipid tails and that there is a “competition” between the tighter cholesterol–lipid packing and the looser lipid–lipid packing as the membrane changes from the  $l_d$  to  $l_o$  phase [66].

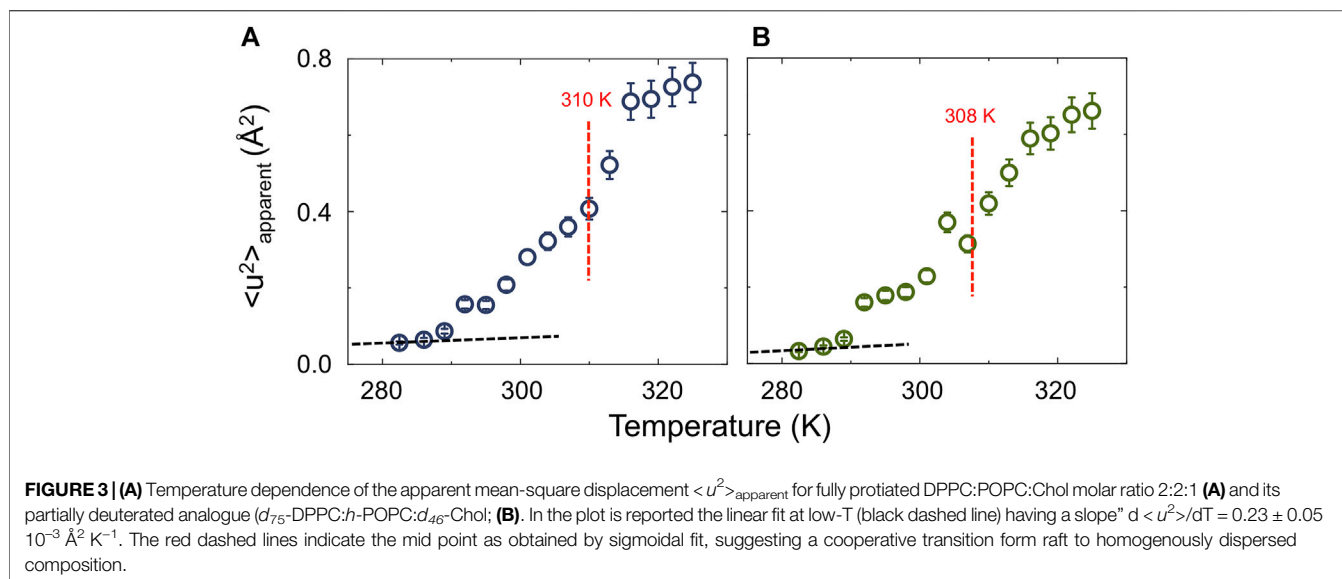
### 3.2 Lipid Dynamics

The dynamics of lipid membranes includes multiple relaxation processes on local and global scales [67–70]. These are associated with motions such as diffusion, shape and thickness fluctuations, membrane undulations, lipid flip-flops, localized rotations, and vibrational motions. Such dynamics thus span a broad range of time and spatial scales [65], and in order to study them one thus needs a technique that will allow the various contributions to be

disentangled, without perturbation. QENS is ideal in this regard as it allows a “serial decoupling” approach (originally introduced by Angell and co-workers for ion-conducting glasses [71, 72], and now extended to technological membranes [73, 74]).

In the studies reported here, the mobility of the lipids comprising the vesicle bilayers was investigated using IRIS (primarily to focus on the lipid lateral diffusion), employing isotopic contrast variation to disentangle how the dynamics of each lipid component varies as a function of its environment. We first studied the elastic fixed window scan (EFWS) of the fully protiated 2:2:1 DPPC:POPC:Chol vesicles and compared this to its perdeuterated analogue, namely  $d_{75}$ -DPPC: $h$ -POPC: $d_{46}$ -Chol, to highlight only the effect of raft formation on POPC dynamics (**Figure 2**).

The EFWS data shown in **Figure 2A**, for DPPC:POPC:Chol 1:1:1 vesicles, reveals that, at temperatures above  $283 \pm 0.1$  K, the elastic intensity ( $\text{Intensity}_{\text{elastic}}$ ) starts to decrease in a linear manner, pointing to a change in the dynamics of the lipids at



the nanoscale, which would be expected if a phase transition in the vesicles occurred. Not surprisingly, the gradient of elastic intensity change seen for the two isotopic forms of DPPC:POPC:Chol 1:1:1 (namely fully protiated DPPC:POPC:Chol and  $d_{75}$ -DPPC: $h$ -POPC: $d_{46}$ -Chol) is different. The change in slope at around 283 K is associated with an increase in either the entire system ( $h$ -DPPC: $h$ -POPC: $h$ -Chol) or just POPC alkyl chain ( $d_{75}$ -DPPC: $h$ -POPC: $d_{46}$ -Chol) mobility. Furthermore, if we consider that the transition temperatures ( $T_m$ ) of the individual lipid constituents POPC and DPPC) are  $\sim 271$  and  $\sim 314$  K, it is evident that the reduction in elastic intensity cannot be simply associated with a single component  $l_o$ - $l_d$  transition. The transition can thus be associated with the structural transition from “raft-containing” membranes to those with “homogeneously mixed” lipids (Figures 2B–G).

Apparent mean-squared displacements ( $\langle u^2 \rangle_{\text{apparent}}$ ) can be calculated from the EFWS data and are plotted as a function of temperature in Figure 3. The calculated Debye-Waller factor (DWF, Eq. 3; Supplementary Figure S1) at low-T, shows a linear temperature dependence with slope  $d \langle u^2 \rangle / dT = 0.23 \pm 0.05 \times 10^{-3} \text{\AA}^2 \text{K}^{-1}$ . The strong reduction of DWF seen at low-T arises from the macroscopic stiffening as a consequence of the raft formation which implies a reorganization of the lipid chain as well as a reduction of the surface movements. From Figure 3 it is also evident that following the increase in  $\langle u^2 \rangle_{\text{apparent}}$  it is possible to follow the transition from raft to homogeneously dispersed composition. The fact that the process is describable using a sigmoidal function suggests a cooperative process where the presence of rafts favours the formation of more/larger rafts. The sigmoidal function was centred at around 310 K, consistent with the SANS data which indicates rafts at  $\sim 280$  K and a homogenous distribution of the three-components at  $\sim 310$  K.

To gain a detailed insight into the effect of raft formation on the dynamical behaviour of the membrane lipids, QENS experiments were performed at a range of temperatures between  $283$  and  $323 \pm 0.1$  K for the two samples discussed

up to now (the data for  $D_2O$  are reported in Supplementary Figure S2). Furthermore, we extended our study to vesicles prepared with a 1:1:1 molar ratio of  $d_{75}$ -DPPC: $h$ -DOPC: $d_7$ -Chol, to study the effects of raft dimensions and lipid unsaturation on the dynamics.

In Figure 4 the scattering profiles of all the isotopic variants of the vesicles investigated by QENS are reported. The  $D_2O$  contribution was weighted and subtracted from the vesicle data to enable highlighting of the QENS broadening due to lipid dynamics.

The QENS data required two Lorentzian components to obtain a good fit to the experimental data (Supplementary Figure S3). Based on the time scale investigated (tens of ps;  $E_{\text{res}} = 17.5 \mu\text{eV}$ ), we associate the narrow component to “in-plane” diffusion, while the broader component is considered to be due to the segmental relaxation of the lipid, following the approach of Sharma *et al.* [54–56]. The “in-plane” diffusion was modelled using the jump diffusion model (Eq. 5, as previously reported [76–79]); the resulting fits are shown in Figure 4 (see Table 2).

Despite the research reported in the literature, very little is known about the mechanism of how lipids diffuse; this is mainly because lipid dynamic behaviour is a complex phenomenon governed by a hierarchy of fluctuations and movements which cover an extremely wide range of correlation times (pico-seconds to seconds [76]). This explains why different experimental techniques, and therefore different time scales, as well as different sample preparations, yield diffusion coefficients that differ by around 2 orders of magnitude [68, 76–83]. For instance, in the case of experiments performed on lipid single-layers on a solid substrate, the diffusion in the lower leaflet is suppressed by the presence of the substrate, while the diffusion in the upper leaflet may be enhanced by a highly ordered fluid phase of the lipids [76]. Similarly, in the case of lipid multi-layer systems, by changing sample orientation (i.e.,  $45^\circ$  vs.  $135^\circ$ ) with respect to the incident beam, it is possible to probe either “out-of-plane” or “in-



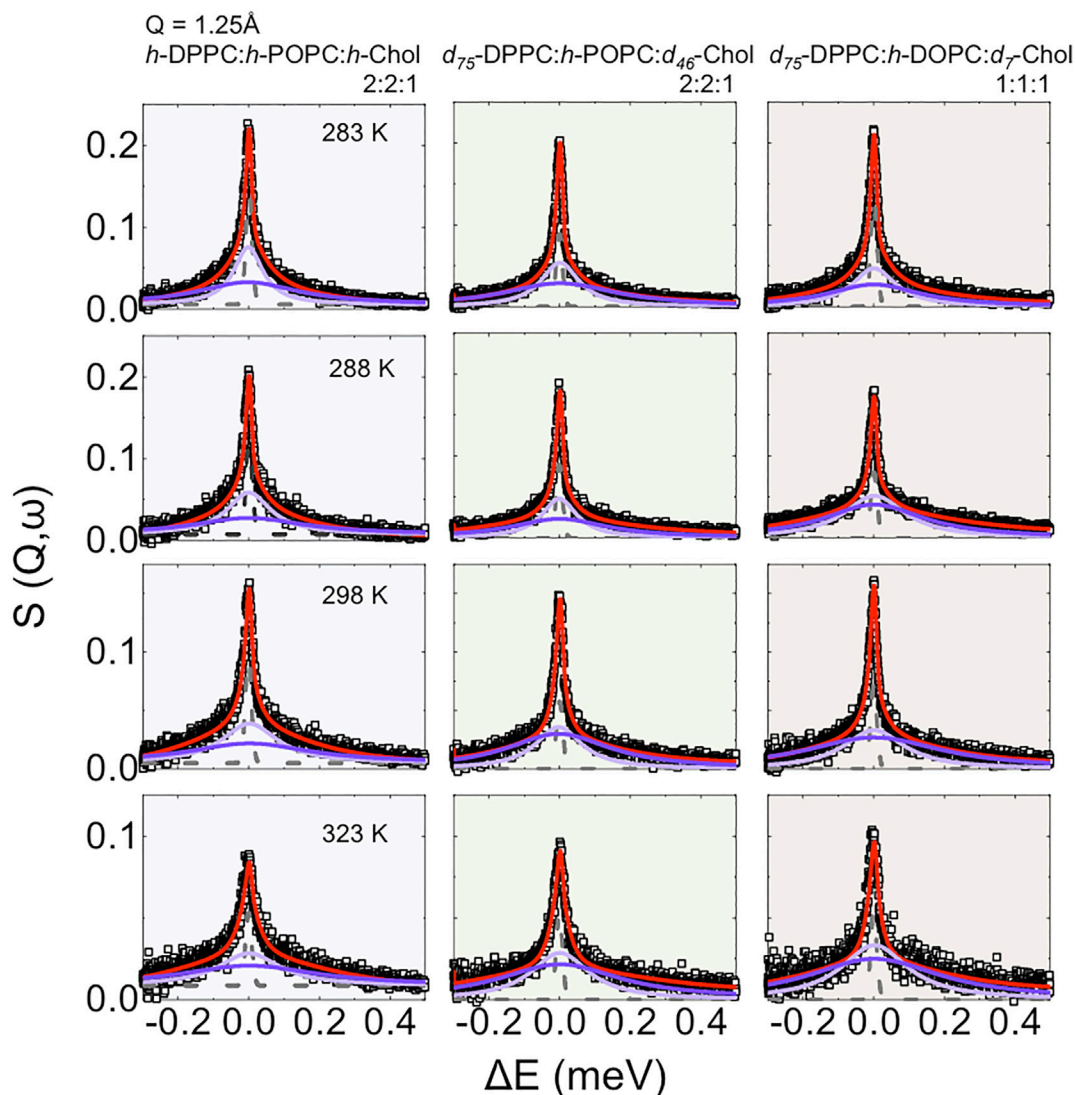
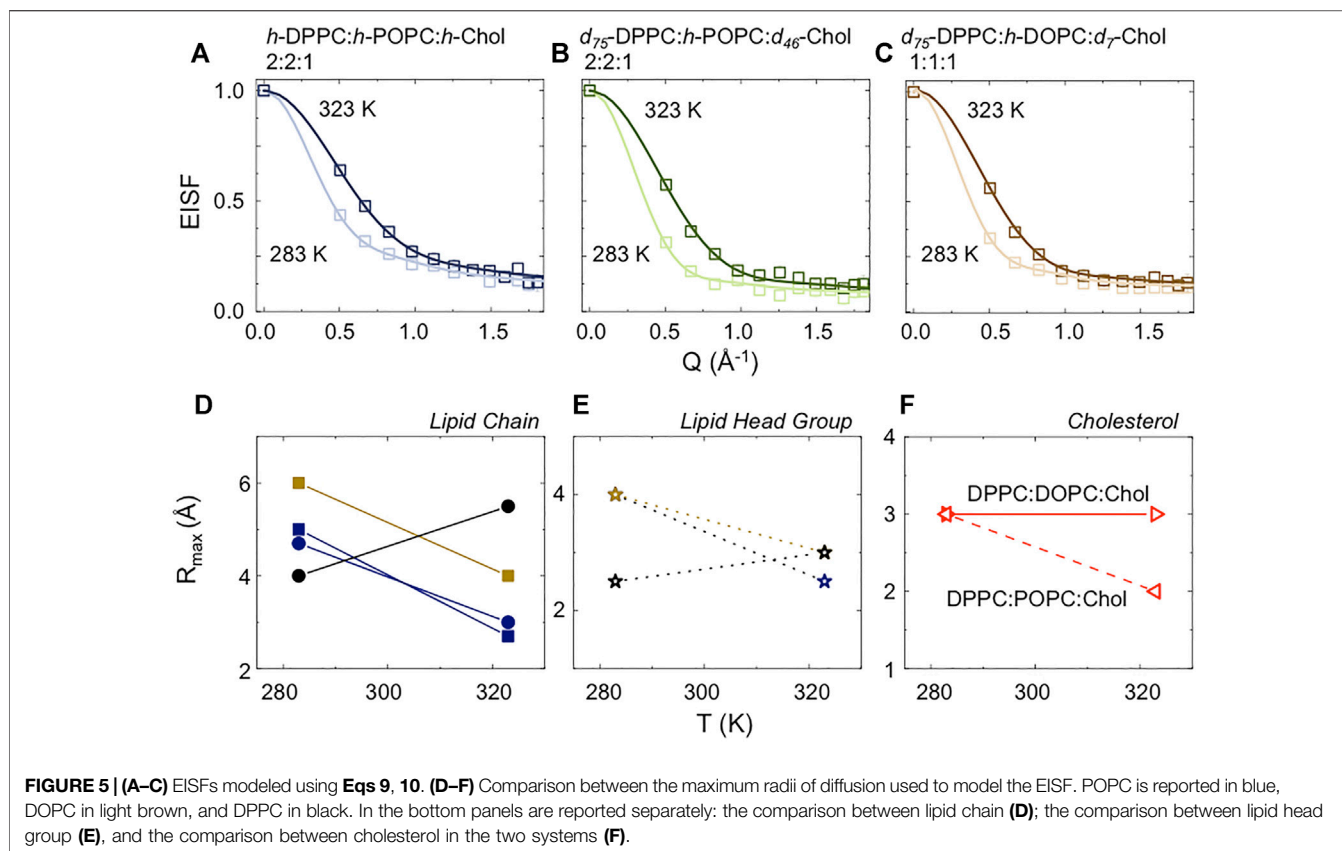


**FIGURE 4** | QENS  $S(Q, \omega)$  data and model fit at a representative value of  $Q = 1.25 \text{ \AA}^{-1}$ , measured on IRIS, with  $17.5 \text{ \mu eV}$  resolution, between 283 and 323 K for: 1)  $h\text{-DPPC}:h\text{-POPC}:h\text{-Chol}$  molar ratio 2:2:1 (in this contrast most of the signal is due to POPC; the other components are virtually “invisible”) and 2)  $d_{75}\text{-DPPC}:h\text{-POPC}:d_{46}\text{-Chol}$  molar ratio 2:2:1 (in this contrast most of the signal is due to POPC; the other components are virtually “invisible”) and 3)  $d_{75}\text{-DPPC}:h\text{-DOPC}:d_7\text{-Chol}$  molar ratio 1:1:1 (in this contrast most of the signal is due to DOPC; the other components are virtually “invisible”). The central line (grey) due to elastic scattering is modeled by the instrumental resolution. The narrow Lorentzian signal (light purple) indicates the lipid diffusion; the broader (dark purple) component represents the lipid segmental relaxation. The global fit (red continuous curve) is overlain on the data points (black open squares).

plane” motion, which results in a different ( $\sim 1$  order of magnitude) self-diffusion coefficient [77–79]. Further, a variation in fluidity of  $\sim 50\%$  was shown by comparing unilamellar and multilamellar phases. This variation in fluidity is associated with the enhanced diffusivity of  $-\text{CH}_2$  in the unilamellar phase, which translates to an increased “in-plane” diffusion [84–86]. In this scenario, and for the data reported here, the enhancement in diffusivity ( $\sim 10^{-6} \text{ cm}^2 \text{ s}^{-1}$ ) might arise as a consequence of the sample preparation—involving use of a pressure extruder. Interestingly, it can be seen from the data for the partially deuterated samples, that POPC/DOPC lateral diffusion *reduces* by around 70% during the heating. Although

this seems at first unexpected, this reduction in diffusion with increasing temperature occurs when the vesicular system converts from phase separated (containing lipid rafts platforms; at 283 K) to homogeneous (at 323 K) states. At the range of experimental temperatures studied, namely between 283 and 323 K, both POPC and DOPC should be in the fluid phase ( $T_m$  of  $\sim 271$  and  $\sim 257$  K, respectively). However, at the higher temperature of 323 K, the lipids in the vesicular bilayer have become homogeneously mixed (no rafts present), thus the DOPC/POPC lipids will interact with the cholesterol that is randomly distributed throughout the vesicle bilayer at this temperature. As a consequence of the cholesterol condensation effect, the POPC/



DOPC dynamics slow down when in the presence of cholesterol. At cooler temperatures, the cholesterol is effectively confined to DPPC-rich rafts, and thus interacts little with the DOPC/POPC lipids present in the disordered regions. This result is in agreement with the earlier findings of Sarangi *et al.* who reported a similar decrease in lipid diffusivity ( $\sim 75\%$ ) upon movement from Chol-poor to Chol-rich regions in POPC-Chol lipid bilayers [21].

In the case of the fully protiated sample a more complicated situation must be considered. Upon heating, the lateral diffusion is seen to reduce by approximately 40%. This result is a consequence of two simultaneous phenomena occurring, namely a decrease in the mobility of the POPC, but an increase in the mobility of DPPC as the temperature increases. The decrease in the mobility of the POPC occurs because, as previously described, it is exposed to a higher concentration of cholesterol when the rafts break down, whereas the mobility of the DPPC increases as the temperature rises above its  $T_m$  ( $\sim 314$  K) and as the break down of the rafts, and associated redistribution of the cholesterol in the system effectively lowers the concentration of cholesterol in the local environment of the DPPC. This reduction in mobility also agrees with the findings from previous NMR studies [87]. Our interpretation of the QENS data is in agreement with experimental and MD simulation data, indicating that cholesterol in the  $l_o$  phase mixes ideally with POPC, whilst also having a strong attraction for DPPC. In the  $l_d$  phase, on the other hand, it mixes ideally with DPPC while exhibiting a significant repulsion for POPC [66, 88, 89].

Furthermore, despite the interactions between DPPC and POPC being neither attractive nor repulsive in the  $l_o$  phase, in the  $l_d$  phase these become repulsive [66, 90].

To better investigate this phenomenon, we carefully analyzed the EISF (Table 3; Figure 5) to characterize the mobility of the single lipid chains in the entire set of investigated samples. Our results at 283 K indicate that the POPC/DOPC are in their “fluid phase” (low-T and low cholesterol concentration) with an organization in agreement with literature data [90–93]. We further notice that DOPC has a slightly higher ( $\sim 10\%$ ) mobility than POPC (Figure 5D, squares). This could be due to a “synchronous” effect of: 1) a difference in  $T_m$  between the two lipids; as well as, more importantly, 2) the presence of cholesterol in the system and 3) its different interaction with POPC vs. DOPC. Indeed, the calculations performed by Pandit *et al.* [65], suggest a reduced partial molecular area for cholesterol in the presence of POPC, compared to cholesterol in the presence of DOPC. These authors indicate that a possible reason for such enhanced packing, is a “special arrangement” in the POPC bilayer in which the  $\alpha$ -face (smooth side) of cholesterol packs around the saturated chain, while the  $\beta$ -face (methylated side) packs well around the unsaturated chain, resulting in a better packing around cholesterol or neighboring lipids [94]. The data for DPPC suggest a more compact configuration ( $\sim 30\%$ ), as also clearly demonstrated by the sharper decrease of the elastic line in the fully protiated sample (Figure 2A, blue triangles), which is remarkably independent from the sample composition (Figure 5D, black

**TABLE 2** | Dynamical properties extracted from the fits as a function of temperature (from 283 to 323 K) for *h-DPPC:h-POPC:h-Chol* molar ratio 2:2:1; *d<sub>75</sub>-DPPC:h-POPC:d<sub>46</sub>-Chol* molar ratio 2:2:1 and *d<sub>75</sub>-DPPC:h-DOPC:d<sub>7</sub>-Chol* molar ratio 1:1:1. In the fully protiated sample the scattering profile is the result of the “sum” of each component’s dynamics (appropriately weighted). The partially deuterated samples are virtually “invisible”, therefore, used to only highlight dynamics from the *h*-component (i.e., POPC and DOPC). In these regards the comparison between 2:2:1 composition (e.g. fully protiated and partially deuterated) would highlight only the dynamics of POPC. The comparison between 2:2:1 vs. 1:1:1 composition (both partially deuterated) would highlight the difference in dynamics between POPC and DOPC.

Sample	Temperature (K)	$D_{tr\_jump} 10^{-5} (cm^2s^{-1})$	$\tau_0$ (ps)
<i>d<sub>75</sub>-DPPC:h-DOPC:d<sub>7</sub>-Chol</i> 1:1:1	283	0.78	3.5
	288	0.50	4.3
	298	0.39	6.5
	323	0.21	8.9
<i>h-DPPC:h-POPC:h-Chol</i> 2:2:1	283	0.82	5.2
	288	0.78	6.0
	298	0.58	8.2
	323	0.46	10.8
<i>d<sub>75</sub>-DPPC:h-POPC:d<sub>46</sub>-Chol</i> 2:2:1	283	0.71	4.6
	288	0.63	5.6
	298	0.27	7.0
	323	0.18	9.5
D <sub>2</sub> O	283	1.04	1.8
	288	1.14	1.2
	298	1.70	1.1
	323	2.10	1.0

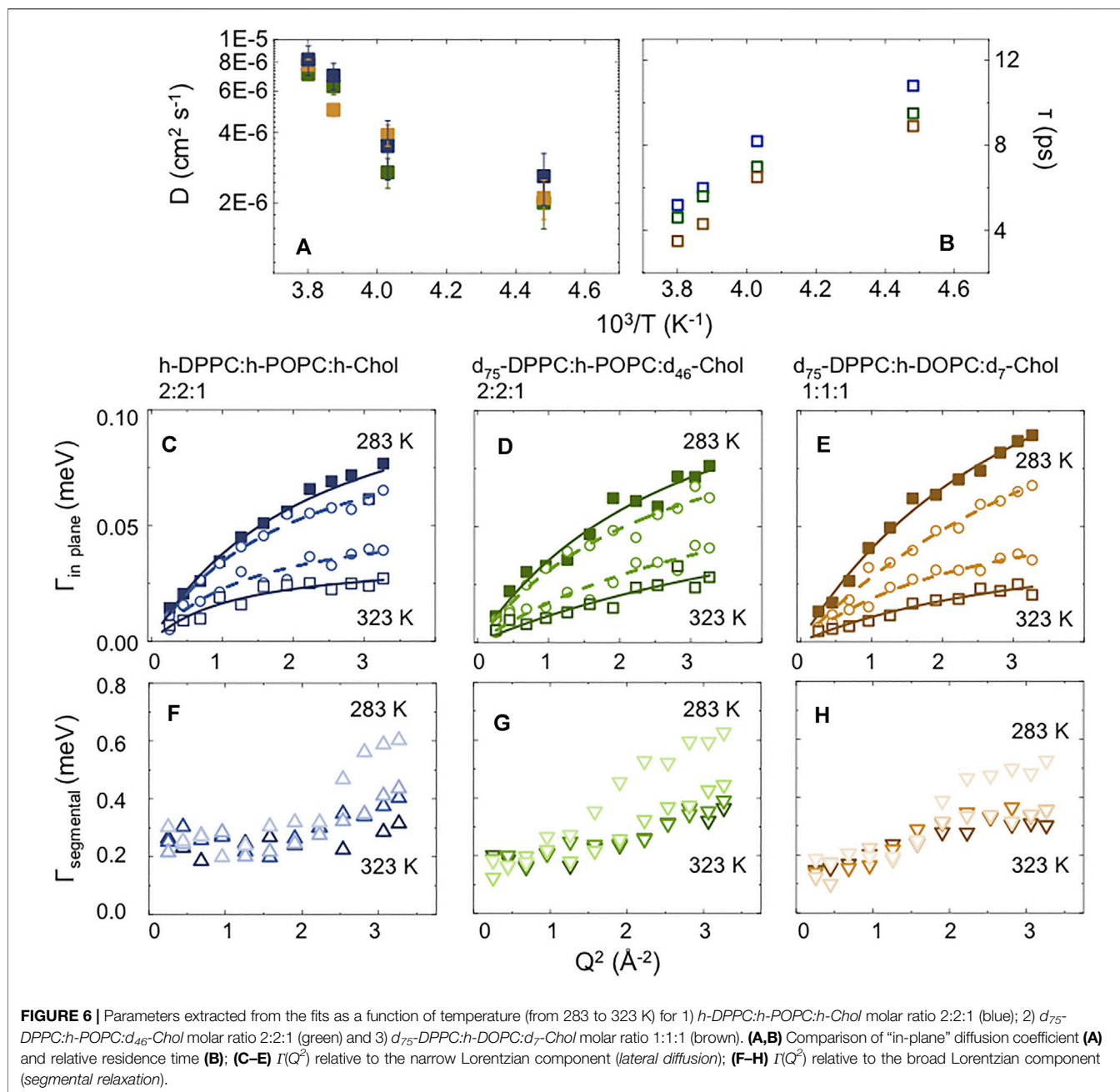
**TABLE 3** | Structural parameters obtained from EISF using Eqs 9, 10. Errors are ~10%. Each contribution has been weighted for the fraction of mobile hydrogen atoms in the system and then added together. The partially deuterated sample was first analysed, to only model POPC, and then these parameters were constrained in the case of the fully protiated sample to best describe DPPC and cholesterol.

Sample	Temperature (K)	Lipid	Chain 1 (Å)	Chain 2 (Å)	Head Group (Å)
<i>d<sub>75</sub>-DPPC:h-DOPC:d<sub>7</sub>-Chol</i>	283	DOPC	0.2	—	0.2
			6.0	—	4.0
		DPPC	0.2	—	0.2
			4.0	—	2.5
		Chol	2.5	—	—
			3.0	—	—
	323	DOPC	0.2	—	0.2
			4.0	—	3.0
		DPPC	0.2	—	0.2
			5.5	—	3.0
		Chol	2.5	—	—
			3.0	—	—
<i>h-DPPC:h-POPC:h-Chol</i> / <i>d<sub>75</sub>-DPPC:h-POPC:d<sub>46</sub>-Chol</i>	283	POPC	0.2	0.2	0.2
			5.0	4.7	4.0
		DPPC	0.2	—	0.2
			4.0	—	2.5
		Chol	2.5	—	—
			3.0	—	—
	323	POPC	0.2	0.2	0.2
			2.7	3.0	2.5
		DPPC	0.2	—	0.2
			5.5	—	2.5
		Chol	2.5	—	—
			2.0	—	—

filled circles). This finding is not surprising as DPPC is an integral part of the raft platform at 283 K.

A different scenario arises when the temperature is increased to 323 K. In this case the conversion from “raft-containing” to

“homogeneous” vesicles leads to a “redistribution” of cholesterol within the system; this in turn leads to an increase of the DPPC mobility and a reduction in the mobility of the POPC and DOPC. Unsurprisingly the mobility of cholesterol at high-T, is dependent



upon the vesicle membrane composition (around -30%, comparing molar ratio 1:1:1 vs. 2:2:1; **Figure 6F**) and agrees with the model presented by Pandit et al. [65], who suggested that the presence of POPC causes a reduction in the partial molecular area for cholesterol as a consequence of “more effective” packing.

## 4 CONCLUSION

The SANS data recorded show that lipid mixtures 1:1:1 DPPC:DOPC:cholesterol and 2:2:1 DPPC:POPC:cholesterol form

homogeneous dispersions absent of any lipid rafts at 308 K, while at 279 K lipid rafts of ~18 and ~7 nm diameter are formed, in agreement with the nanometre-sized structures previously reported in the literature and consistent with the idea that larger rafts are formed when there is a greater mis-match in lipids, i.e. DPPC/DOPC compared to DPPC/POPC [24, 31]. To learn more about the dynamics of the lipids within these different phases, we have used QENS to characterise the “in-plane” diffusion as well as the lipid segmental relaxations. The elastic incoherent structure factor was used to extract the extent of mobility of the various lipid species within the mixture and confirms the better packing between Chol-

PC as well as PC-PC [65, 66, 88–95] at high temperature, as a consequence of a homogenous distribution of the components in the system. The data indicate that upon cooling, the formation of lipid rafts rich in DPPC and Chol, is co-operative. Upon warming of the samples the translation diffusion is found to decrease. Analysis of the different components in the DPPC:POPC:Chol mixtures shows that this can be attributed to an increase in mobility of the DPPC as the temperature increases with an associated decrease in the mobility of the POPC. The increase in mobility of the DPPC is attributed not just to warming the lipid above its  $T_m$  but also to the lowering of the cholesterol concentration around the DPPC caused by the breakdown of the lipid rafts and consequent redistribution of the cholesterol in the membrane. In the case of POPC a decrease in mobility of around 70% occurs as it goes from being exposed to little cholesterol at low temperatures, as the cholesterol is sequestered into rafts with the DPPC, to being in a relatively cholesterol rich environment when the rafts break down, and the cholesterol reduces its mobility. Thus, the changes in the diffusion of the system reflect the distribution of the cholesterol, provides information on how cholesterol changes the diffusion of lipids within bilayers, and highlights the importance of the local environment on lipid diffusion.

We have thus shown here how the temperature-induced phase separation in model membrane systems can be explored without the need to incorporate any labelled reporter molecule (as, of necessity, required in fluorescence/confocal microscopy studies, for example), using SANS to afford an estimate of the mean sizes of the lipid domains, and QENS to provide detail on the lipid diffusional behavior. Given that phase segregated model membranes of the type studied here can be used to mimic the lipid lateral heterogeneity present in the plasma membranes of cells, these tools might in future be used to study the lipid dynamics in disease-relevant systems in a controlled and non-perturbing fashion *in vitro*.

## DATA AVAILABILITY STATEMENT

The datasets presented in this study can be found in online repositories. The names of the repository/repositories and accession number(s) can be found below: doi:10.5286/ISIS.E.RB1720338 doi:10.5291/ILL-DATA.9-13-722.

## AUTHOR CONTRIBUTIONS

MJL and KCT initiated the study in close collaboration with DJB. FF devised the programme of QENS experiments and carried out

all data analysis; DJB carried out all SANS data analysis. MM, MH, VTF, GAS, and HP produced the perdeuterated cholesterol used in the neutron experiments. FF and DA prepared the samples and participated in neutron experiments along with MJL, DJB, and KCT. VGS and RS enabled access to beamline experiments at both facilities and participated in experiments and interpretation of results. All authors contributed to the preparation of the manuscript.

## FUNDING

FF would like to acknowledge the EPSRC (grant EP/V057863/1) for funding. VTF, MH, MJL, and DJB acknowledge the EPSRC for grants EP/C015452/1 and GR/R99393/01 that funded the creation of the Deuteration Laboratory in the Life Sciences Group at the Institut Laue-Langevin/Partnership for Structural Biology. This work benefited from the use of the SasView application, originally developed under NSF award DMR-0520547. SasView contains code developed with funding from the European Union's Horizon 2020 research and innovation programme under the SINE2020 project, grant agreement No. 654000.

## ACKNOWLEDGMENTS

We thank ISIS (Didcot, United Kingdom) for beam-time on IRIS under proposal number 1720338 (doi:10.5286/ISIS.E.RB1720338) and for financial support for experimental consumables (Grant RB 1720338). We are grateful to the Institut Laue Langevin (Grenoble, France) for neutron beam-time on D11 under proposal number 9-13-722 (doi:10.5291/ILL-DATA.9-13-722) as well as for accessing fully deuterated cholesterol (Grant DL-03-202). FF would like to acknowledge the EPSRC (grant EP/V057863/1) for funding. VTF, MH, MJL, and DJB acknowledge the EPSRC for grants EP/C015452/1 and GR/R99393/01 that funded the creation of the Deuteration Laboratory in the Life Sciences Group at the Institut Laue-Langevin/Partnership for Structural Biology.

## SUPPLEMENTARY MATERIAL

The Supplementary Material for this article can be found online at: <https://www.frontiersin.org/articles/10.3389/fphy.2022.864746/full#supplementary-material>

## REFERENCES

1. Shan Y, Wang H. The Structure and Function of Cell Membranes Examined by Atomic Force Microscopy and Single-Molecule Force Spectroscopy. *Chem Soc Rev* (2015) 44(11):3617–38. doi:10.1039/c4cs00508b
2. Silvius JR. Role of Cholesterol in Lipid Raft Formation: Lessons from Lipid Model Systems. *Biochim Biophys Acta (Bba) - Biomembranes* (2003) 1610(2):174–83. doi:10.1016/s0005-2736(03)00016-6
3. Karnovsky MJ, Kleinfeld AM, Hoover RL, Klausner RD. The Concept of Lipid Domains in Membranes. *J Cel Biol* (1982) 94:1–6. doi:10.1083/jcb.94.1.1
4. Brown DA, London E. Functions of Lipid Rafts in Biological Membranes. *Annu Rev Cel Dev. Biol.* (1998) 14(1):111–36. doi:10.1146/annurev.cellbio.14.1.111

5. Alonso MA, Milla'n J. The Role of Lipid Rafts in Signalling and Membrane Trafficking in T Lymphocytes. *J Cel Sci* (2001) 114(22):3957–65. doi:10.1242/jcs.114.22.3957
6. Quinn PJ, Wolf C. The Liquid-Ordered Phase in Membranes. *Biochim Biophys Acta (Bba) - Biomembranes* (2009) 1788:33–46. doi:10.1016/j.bbamem.2008.08.005
7. Radakrishnan A, Anderson TG, McConnell HM. Condensed Complexes, Rafts, and the Chemical Activity of Cholesterol in Membranes. *Proc Natl Acad Sci United States America* (2000) 97:12422–7.
8. Anderson TG, McConnell HM. Condensed Complexes and the Calorimetry of Cholesterol-Phospholipid Bilayers. *Biophysical J* (2001) 81:2774–85. doi:10.1016/s0006-3495(01)75920-6
9. Goñi FM. Rafts<sup>+</sup>: A Nickname for Putative Transient Nanodomains. *Chem Phys Lipids* (2019) 218:34–9.
10. Lu SM, Fairn GD. Mesoscale Organization of Domains in the Plasma Membrane - beyond the Lipid Raft. *Crit Rev Biochem Mol Biol* (2018) 53(2):192–207. doi:10.1080/10409238.2018.1436515
11. Sezgin E, Levental I, Mayor S, Eggeling C. The Mystery of Membrane Organization: Composition, Regulation and Roles of Lipid Rafts. *Nat Rev Mol Cel Biol* (2017) 18:361–74. doi:10.1038/nrm.2017.16
12. Germain V, Perraki A, Mongrand S. *Lipid Rafts*. eLS (2012).
13. Adhyapak P, Kapoor S. Membrane Dynamics in Health and Disease: Impact on Cellular Signalling. *J Membr Biol* (2019) 252:213–26. doi:10.1007/s00232-019-00087-0
14. Bagam P, Singh DP, Inda ME, Batra S. Unraveling the Role of Membrane Microdomains during Microbial Infections. *Cell Biol Toxicol* (2017) 33:429–55. doi:10.1007/s10565-017-9386-9
15. Morgan PK, Fang L, Lancaster GI, Murphy AJ. Hematopoiesis Is Regulated by Cholesterol Efflux Pathways and Lipid Rafts: Connections with Cardiovascular Diseases. *J Lipid Res* (2020) 61(5):667–75. doi:10.1194/jlr.tr119000267
16. Grassi S. Lipid Rafts and Neurodegeneration: Structural and Functional Roles in Physiologic Aging and Neurodegenerative Diseases. *J Lipid Res* (2020) 61(5): 636–54. doi:10.1194/jlr.tr119000427
17. Fang L, Miller YI. Regulation of Lipid Rafts, Angiogenesis and Inflammation by AIBP. *Curr Opinions Lipidol* (2019) 30(3):218–23. doi:10.1097/mol.0000000000000596
18. Vona R, Iessi E, Matarrese P. Role of Cholesterol and Lipid Rafts in Cancer Signaling: A Promising Therapeutic Opportunity? *Front Cel Dev Biol* (2021) 9: 622908. doi:10.3389/fcell.2021.622908
19. Murai T. The Role of Lipid Rafts in Cancer Cell Adhesion and Migration. *Int J Cel Biol* (2012) 2012:763283. doi:10.1155/2012/763283
20. Zalba S, ten Hagen TL. Cell Membrane Modulation as Adjuvant in Cancer Therapy. *Cancer Treat Rev* (2017) 52:48–57. doi:10.1016/j.ctrv.2016.10.008
21. Sarangi NK, Ayappa KG, K Basu J. Complex Dynamics at the Nanoscale in Simple Biomembranes. *Scientific Rep* (2017) 7:11173. doi:10.1038/s41598-017-11068-5
22. Lozano MM, Hovis JS, Moss FR, III, Boxer SG. Dynamical Reorganization and Correlation Among Lipid Raft Components. *J Am Chem Soc* (2016) 138: 9996–10001. doi:10.1021/jacs.6b05540
23. Schafera LV. Lipid Packing Drives the Segregation of Transmembrane Helices into Disordered Lipid Domains in Model Membranes. *Proc Natl Acad Sci United States America* (2011) 108(4):1343–8.
24. Nickels JD. Mechanical Properties of Nanoscopic Lipid Domains. *J Am Chem Soc* (2015) 137:15772–80. doi:10.1021/jacs.5b08894
25. Bolmatov D. Molecular Picture of the Transient Nature of Lipid Rafts. *Langmuir* (2020) 36:4887–96. doi:10.1021/acs.langmuir.0c00125
26. Heberle FA. Bilayer Thickness Mismatch Controls Domain Size in Model Membranes. *J Am Chem Soc* (2013) 135:6853–9. doi:10.1021/ja3113615
27. Marquardt D, Heberle FA, Nickels JD, Pabst G, Katsaras J. On Scattered Waves and Lipid Domains: Detecting Membrane Rafts with X-Rays and Neutrons. *Soft Matter* (2015) 11:9055. doi:10.1039/c5sm01807b
28. Kinnun JJ, Bolmatov D, Lavrentovich MO, Katsaras J. Lateral Heterogeneity and Domain Formation in Cellular Membranes. *Chem Phys Lipids* (2020) 232: 104976. doi:10.1016/j.chemphyslip.2020.104976
29. Kinnun JJ, Scott HL, Ashkar R, Katsaras J. Biomembrane Structure and Material Properties Studied with Neutron Scattering. *Front Chem* (2021) 9: 642851. doi:10.3389/fchem.2021.642851
30. Scherfeld D, Kahya N, Schwille P. Lipid Dynamics and Domain Formation in Model Membranes Composed of Ternary Mixtures of Unsaturated and Saturated Phosphatidylcholines and Cholesterol. *Biophysical J* (2003) 85: 3758–68. doi:10.1016/s0006-3495(03)74791-2
31. Pencer J. Detection of Submicron-Sized Raft-like Domains in Membranes by Small-Angle Neutron Scattering. *The Eur Phys J E* (2005) 18:447–58. doi:10.1140/epje/e2005-00046-5
32. Bag N, Yap DHX, Wohland T. Temperature Dependence of Diffusion in Model and Live Cell Membranes Characterized by Imaging Fluorescence Correlation Spectroscopy. *Biochim Biophys Acta* (20142005) 183818: 802447–13458. doi:10.1016/j.bbamem.2013.10.009
33. Bacia K, Scherfeld D, Kahya N, Schwille P. Fluorescence Correlation Spectroscopy Relates Rafts in Model and Native Membranes. *Biophysical J* (2004) 87(2):1034–43. doi:10.1529/biophysj.104.040519
34. de Almeida R, Fedorov A, Prieto M. Sphingomyelin/phosphatidylcholine/cholesterol Phase Diagram: Boundaries and Composition of Lipid Rafts. *Biophysical J* (2003) 85(4):2406–16. doi:10.1016/s0006-3495(03)74664-5
35. de Almeida R, Loura L, Fedorov A, Prieto M. Lipid Rafts Have Different Sizes Depending on Membrane Composition: a Time-Resolved Fluorescence Energy Transfer Study. *J Mol Biol* (2005) 346(4):1109–20. doi:10.1016/j.jmb.2004.12.026
36. Keller S, Anderson T, McConnell H. Miscibility Critical Pressures in Monolayers of Ternary Lipid Mixtures. *Biophysical J* (2000) 79(4):2033–42. doi:10.1016/s0006-3495(00)76451-4
37. Stottrup B, Veatch S, Keller S. Nonequilibrium Behavior in Supported Lipid Membranes Containing Cholesterol. *Biophysical J* (2004) 86(5):2942–50. doi:10.1016/s0006-3495(04)74345-3
38. Rondelli V. Neutrons for Rafts, Rafts for Neutrons. *Eur Phys J E* (2013) 36:73. doi:10.1140/epje/i2013-13073-4
39. Haertlein M. Biomolecular Deuteration for Neutron Structural Biology and Dynamics. *Methods Enzymol* (2016) 566:113–57. doi:10.1016/bs.mie.2015.11.001
40. Hinz M, Richter G, Leitner E, Wriessnegger T, Pichler H. A Novel Cholesterol-Producing *Pichia pastoris* Strain Is an Ideal Host for Functional Expression of Human Na,K-ATPase  $\alpha 3\beta 1$  Isoform. *Appl Microbiol Biotechnol* (2013) 97(21): 9465–78. doi:10.1007/s00253-013-5156-7
41. Moulin M. Perdeuteration of Cholesterol for Neutron Scattering Applications Using Recombinant *Pichia pastoris*. *Chem Phys Lipids* (2018) 212:80–7. doi:10.1016/j.chemphyslip.2018.01.006
42. Waldie S. The Production of Matchout-Deuterated Cholesterol and the Study of Bilayer-Cholesterol Interactions. *Scientific Rep* (2019) 9:5118. doi:10.1038/s41598-019-41439-z
43. Waldie S. Localization of Cholesterol within Supported Lipid Bilayers Made of a Natural Extract of Tailor-Deuterated Phosphatidylcholine. *Langmuir* (2018) 34(1):472–9. doi:10.1021/acs.langmuir.7b02716
44. Lindner P, Schweins R. The D11 Small-Angle Scattering Instrument: A New Benchmark for SANS. *Neutron News* (2010) 21(2):15–8. doi:10.1080/10448631003697985
45. LAMP, the Large Array Manipulation Program. *LAMP, the Large Array Manipulation Program* (1996).
46. Doucet M. *SasView Version 4.2*. Zenodo (2018).
47. Campbell SI, Telling MTF, Carlile CJ. The Optimisation of Analyser Geometry in Near-Backscattering Spectrometers – IRIS on the ISIS-Pulsed Source. *Physica B: Condensed Matter* (2000) 276-278:206–7. doi:10.1016/s0921-4526(99)01286-7
48. Arnold O. Mantid - Data Analysis and Visualization Package for Neutron Scattering and  $\mu$ SR Experiments. *Nucl Instr Methods Phys Res Section A* (2014) 764:156–66. doi:10.1016/j.nima.2014.07.029
49. Bée M. *Quasielastic Neutron Scattering: Principles and Applications in Solid State Chemistry, Biology and Material Science*. Bristol: Adam Hilger (1988).
50. Teixeira J, Bellissent-Funel M-C, Chen S-H, Dianoux AJ. Experimental Determination of the Nature of Diffusive Motions of Water Molecules at Low Temperatures. *Phys Rev A* (1985) 31:1913–7. doi:10.1103/physrev.31.1913
51. Sears VF. Theory of Cold Neutron Scattering by Homonuclear Diatomic Liquids: I. Free Rotation. *Can J Phys* (1996) 44:1279–97.
52. Sears VF. Cold Neutron Scattering by Molecular Liquids: II. Methane. *Can J Phys* (1996) 44:1299–311.
53. Singwi K, Sjölander A. Resonance Absorption of Nuclear Gamma Rays and the Dynamics of Atomic Motions. *Phys Rev* (1960) 120(4):1093. doi:10.1103/physrev.120.1093

54. Sharma VK, Ghosh SK, García Sakai V, Mukhopadhyay R. Enhanced Microscopic Dynamics of a Liver Lipid Membrane in the Presence of an Ionic Liquid. *Front Chem* (2020) 8:577508. doi:10.3389/fchem.2020.577508
55. Sharma VS, Mamontov E, Anunciado DB, O'Neill H, Urban V. Nanoscopic Dynamics of Phospholipid in Unilamellar Vesicles: Effect of Gel to Fluid Phase Transition. *J Phys Chem B* (2015) 119:4460–70. doi:10.1021/acs.jpcc.5b00220
56. Sharma VK, Mamontov E, Anunciado DB, O'Neill H, Urban VS. Effect of Antimicrobial Peptide on the Dynamics of Phosphocholine Membrane: Role of Cholesterol and Physical State of Bilayer† Check for Updates. *Soft Matter* (2015) 11:6755–67. doi:10.1039/c5sm01562f
57. Volino F, Dianoux A. Neutron Incoherent Scattering Law for Diffusion in a Potential of Spherical Symmetry: General Formalism and Application to Diffusion inside a Sphere. *Mol Phys* (1980) 41:271–9. doi:10.1080/0026897800102761
58. Carpentier L, Bée M, Giroud-Godquin AM, Maldivi P, Marchon JC. Alkyl Chain Motions in Columnar Mesophases. *Mol Phys* (1989) 68:1367. doi:10.1080/00268978900102971
59. Bokuchava GD, Gorshkova YE. Analysis of Small Angle Neutron Scattering from Nanocrystalline Niobium Carbide Powders Using Global Scattering Functions. *J Optoelectronics Adv Mater* (2015) 17(7):985–90.
60. Su TJ, Lu JR, Cui ZF, Thomas RK, Heenan RK. Application of Small Angle Neutron Scattering to the *In Situ* Study of Protein Fouling on Ceramic Membranes. *Langmuir* (1998) 14:5517–20. doi:10.1021/la980392b
61. Schmidt PW. Small-angle X-ray Scattering from the Surfaces of Reversed-phase Silicas: Power-Law Scattering Exponents of Magnitudes Greater Than Four. *J Chem Phys* (1991) 94:1474–9. doi:10.1063/1.460006
62. Hammouda B. A New Guinier-Porod Model. *J Appl Crystallogr* (2010) 43:716–9. doi:10.1107/s0021889810015773
63. Usery RD. Line Tension Controls Liquid-Disordered + Liquid-Ordered Domain Size Transition in Lipid Bilayers. *Biophysical J* (2017) 112:1431–43. doi:10.1016/j.bpj.2017.02.033
64. Zhao L. Phase Studies of Model Biomembranes: Macroscopic Coexistence of La + Lβ, with Light-Induced Coexistence of La + Lo Phases. *Biochim Biophys Acta* (2007) 1768:2777–86. doi:10.1016/j.bbame.2007.07.009
65. Pandit SA, Chiu S-W, Jakobsson E, Grama A, Scott HL. Cholesterol Packing Around Lipids with Saturated and Unsaturated Chains: A Simulation Study. *Langmuir* (2008) 24(13):6858–65. doi:10.1021/la8004135
66. Yang J, Martí J, Calero C. Pair Interactions Among Ternary DPPC/POPC/cholesterol Mixtures in Liquid-Ordered and Liquid-Disordered Phases. *Soft Matter* (2016) 12:4557–61. doi:10.1039/c6sm00345a
67. Qian S, Sharma VK, Clifton LA. Understanding the Structure and Dynamics of Complex Biomembrane Interactions by Neutron Scattering Techniques. *Langmuir* (2020) 36:15189–211. doi:10.1021/acs.langmuir.0c02516
68. Tocanne JF, Dupou-Cézanne L, Lopez A. Lateral Diffusion of Lipids in Model and Natural Membranes. *Prog Lipid Res* (1994) 33(3):203–37. doi:10.1016/0163-7827(94)90027-2
69. Dufourc EJ. Sterols and Membrane Dynamics. *J Chem Biol* (2008) 1(1–4):63–77. doi:10.1007/s12154-008-0010-6
70. Gupta S, De Mel JU, Schneider GJ. Dynamics of Lposomes in the Fluid Phase. *Curr Opin Colloid Interf Sci* (2019) 42:121–36. doi:10.1016/j.cocis.2019.05.003
71. Torell LM, Angell CA. Ion-matrix Coupling in Polymer Electrolytes from Relaxation Time Studies. *Br Polym J* (1988) 20:173–9. doi:10.1002/pi.4980200303
72. Angell CA. Relaxation in Liquids, Polymers and Plastic Crystals - strong/fragile Patterns and Problems. *J Non-Crystalline Sol* (1991) 131-133:13–31. doi:10.1016/0022-3093(91)90266-9
73. Foglia F, García Sakai V, Lyonnard S, McMillan PF. Decoupling Polymer, Water and Ion Transport Dynamics in Ion-Selective Membranes for Fuel Cell Applications. *J Non-Crystalline Sol X* (2022) 13 100073. doi:10.1016/j.nocx.2021.100073
74. Foglia F. Disentangling Water, Ion and Polymer Dynamics in an Anion Exchange Membrane. *Nat Mater* (2022). doi:10.1038/s41563-022-01197-2
75. Humphrey W, Dalke A, Schulten K. VMD - Visual Molecular Dynamics. *J Mol Graphics* (1996) 14:33–8. doi:10.1016/0263-7855(96)00018-5
76. König S, Pfeiffer W, Bayerl T, Richter D, Sackmann E. Molecular Dynamics of Lipid Bilayers Studied by Incoherent Quasi-Elastic Neutron Scattering. *J de Physique* (1992) 2:1589.
77. Pfeiffer W, Henkel T, Sackmann E, Knoll W, Richter D. Local Dynamics of Lipid Bilayers Studied by Incoherent Quasi-Elastic Neutron Scattering. *Europhysics Lett* (1989) 8(2):201–6. doi:10.1209/0295-5075/8/2/016
78. Buchsteiner A, Hauß T, Dante S, Dencher N. Alzheimer's Disease Amyloid-β Peptide Analogue Alters the Ps-Dynamics of Phospholipid Membranes. *Biochim Biophys Acta - Biomembranes* (2010) 1798:1969–76. doi:10.1016/j.bbame.2010.06.024
79. Armstrong CL. Diffusion in Single Supported Lipid Bilayers Studied by Quasi-Elastic Neutron Scattering. *Soft Matter* (2010) 6:5864–7. doi:10.1039/c0sm00637h
80. Falck E, Rög T, Karttunen M, Vattulainen I. Molecular Mechanism of Long-Range Diffusion in Phospholipid Membranes Studied by Quasielastic Neutron Scattering. *J Am Chem Soc* (2008) 130:44–5. doi:10.1021/ja7103558
81. Busch S, Smuda C, Pardo LC, Unruh T. Molecular Mechanism of Long-Range Diffusion in Phospholipid Membranes Studied by Quasielastic Neutron Scattering. *J Am Chem Soc* (2010) 132:3232–3. doi:10.1021/ja907581s
82. Vaz WL, Almeida PF. Microscopic versus Macroscopic Diffusion in One-Component Fluid Phase Lipid Bilayer Membranes. *Biophys J* (1991) 60:1553. doi:10.1016/s0006-3495(91)82190-7
83. Vattulainen I, Mouritsen OG. In: P Heitjans J Kärgel, editors. *Diffusion in Condensed Matter*. Berlin: Springer-Verlag (2005). p. 471–509.
84. Andreozzi P. Multi- to Unilamellar Transitions in Catanionic Vesicles. *J Phys Chem B* (2010) 114:8056–60. doi:10.1021/jp100437v
85. Mitra S. Enhancement of Lateral Diffusion in Catanionic Vesicles during Multilamellar-To-Unilamellar Transition. *J Phys Chem B* (2016) 120:3777–84. doi:10.1021/acs.jpcc.6b02997
86. Orädd G, Westerman PW, Lindblom G. Lateral Diffusion Coefficients of Separate Lipid Species in a Ternary Raft-Forming Bilayer: A PFG-NMR Multinuclear Study. *Biophysical J* (2005) 89:315–20.
87. Bartels T, Lankalapalli RS, Bittman R, Beyer K, Brown MF. Raftlike Mixtures of Sphingomyelin and Cholesterol Investigated by Solid-State 2H NMR Spectroscopy. *J Am Chem Soc* (2008) 130:14521–32. doi:10.1021/ja801789t
88. Krause MR, Daly TA, Almeida PF, Regen SL. Push-Pull Mechanism for Lipid Raft Formation. *Langmuir* (2014) 30:3285–9. doi:10.1021/la500510s
89. Turkyilmaz S, Almeida PF, Regen SL. Effects of Isoflurane, Halothane and Chloroform on the Interactions and Lateral Organization of Lipids in the Liquid-Ordered Phase. *Langmuir* (2011) 27:14380–5. doi:10.1021/la2035278
90. Wang C, Krause MR, Regen SL. The Structural Role of Cholesterol in Cell Membranes: From Condensed Bilayers to Lipid Rafts. *J Am Chem Soc* (2015) 137:664–6. doi:10.1021/ja5115437
91. Wanderlingh U. Multi-component Modeling of Quasielastic Neutron Scattering from Phospholipid Membranes. *J Chem Phys* (2014) 140:174901. doi:10.1063/1.4872167
92. Nanda H. Relaxation Dynamics of Saturated and Unsaturated Oriented Lipid Bilayers. *Soft Matter* (2018) 14:6119–27. doi:10.1039/c7sm01720k
93. Gu R-X, Baoukina S, Tieleman DP. Phase Separation in Atomistic Simulations of Model Membranes. *J Am Chem Soc* (2020) 142:2844–56. doi:10.1021/jacs.9b11057
94. Nyholm TKM. Impact of Acyl Chain Mismatch on the Formation and Properties of Sphingomyelin-Cholesterol Domains. *Biophysical J* (2019) 117:1577–88. doi:10.1016/j.bpj.2019.09.025
95. Williams JA, Wassall CD, Kemple MD, Wassall SR. An Electron Paramagnetic Resonance Method for Measuring the Affinity of a Spin-Labeled Analog of Cholesterol for Phospholipids. *J Membr Biol* (2013) 246:689–96. doi:10.1007/s00232-013-9586-z

**Conflict of Interest:** The authors declare that the research was conducted in the absence of any commercial or financial relationships that could be construed as a potential conflict of interest.

**Publisher's Note:** All claims expressed in this article are solely those of the authors and do not necessarily represent those of their affiliated organizations, or those of the publisher, the editors and the reviewers. Any product that may be evaluated in this article, or claim that may be made by its manufacturer, is not guaranteed or endorsed by the publisher.

Copyright © 2022 Ahmadi, Thompson, García Sakai, Schweins, Moulin, Haertlein, Strohmeier, Pichler, Forsyth, Barlow, Lawrence and Foglia. This is an open-access article distributed under the terms of the Creative Commons Attribution License (CC BY). The use, distribution or reproduction in other forums is permitted, provided the original author(s) and the copyright owner(s) are credited and that the original publication in this journal is cited, in accordance with accepted academic practice. No use, distribution or reproduction is permitted which does not comply with these terms.